(Received 3 April 2026, Accepted 18 May 2026, Scheduled 27 May 2026)

Design and Analysis of a Novel Miniaturized Multiband Flowerpot-Shaped Patch-Based Dielectric Resonator Antenna for 5GNSS, UMTS, PCS, Wi-Fi5, WiMAX, and NR Sub-6 GHz 5G Applications

Kaushal Patel[1,*] and Falgun Thakkar[2]

[1]*Research Scholar, Gujarat Technological University, Gujarat, India*
[2]*G. H. Patel College of Engineering & Technology, CVM University, Gujarat, India*

ABSTRACT: In this study, a novel miniaturized multiband flowerpot-shaped patch-based cylindrical dielectric resonator antenna (FPS-DRA) is proposed for 5G-enabled GNSS (GPS), UMTS, PCS, Wi-Fi5, WiMAX, and NR 77/78 Sub-6 GHz 5G applications. The proposed antenna prototype operates at 1.54 GHz, 2.01 GHz, 3.23 GHz, 3.95 GHz, and 5.54 GHz for the mentioned applications. It employs a novel low-cost flowerpot-shaped radiating patch underneath a cylindrical dielectric resonator (CDR) made of alumina ceramic (Al_2O_3, $\varepsilon_{DR} = 9.8$) material and is fed by a combined microstrip-line-tapered trapezoidal feedline. Later, a reduced ground plane is used as a reflector on the rear side of the substrate to reduce antenna size. It is made up of a low cost 1.6 mm FR4 laminate sheet ($\varepsilon_r = 4.4$, $\tan\delta = 0.02$) and miniaturized to a physical size of 65×45 mm^2. The parametric analysis was carried out for reflection coefficients (S_{11}-dB) by changing the ground plane width, CDRA radius, and flower petal radius to achieve adequate results. Likewise, this prototype has measured reflection coefficient of < -20 dB for 1.54 GHz (L1-band), < -25 dB for 2.01/3.23 GHz (S-band), < -20 dB for 3.95 GHz (S-band), and 5.54 GHz (C-band), peak gains of 2.01 dBi, 2.05 dBi, 3.02 dBi, 4.85 dBi, and 2.24 dBi for the respective bands along with adequate -10 dB impedance matching bandwidths and stable radiation features in a convincing agreement compared to earlier designs. The proposed prototype is simulated in CST software, assembled, and tested by VNA and an anechoic chamber setup for L1/S/C band applications.

1. INTRODUCTION

Over the past few epochs, dielectric resonator antennas (DRAs) have established a massive demand for cellular, 4G, 5G, satellite, wireless communication networks, and wireless strategy networks, owing to their advantages such as low ohmic losses, high radiation efficiency, miniaturization, retrofitting, low surface-wave loss, excitation simplicity, broad bandwidth, high degree of design freedom, and multiband. In contrast, a microstrip patch antenna (MSA) is suitable for most multiband applications due to its easy design, except for a few demerits, such as low gain, narrow bandwidth, and efficiency reduction owing to conduction loss and surface wave reduction [1–3]. Compared to a microstrip patch antenna (MSA), a DRA offers an inherently broader bandwidth and high radiation efficiency by selecting a suitable dielectric permittivity and offers adequate gain due to low metallic loss [4–6]. Among various dielectric resonator (DR) shapes and geometries, cylindrical DRA (CDRA) is easy to resonate owing to an appropriate aspect ratio [7, 8]. Numerous feeding methods are used for exciting resonators, such as microstrip lines, proximity coupling, coaxial feed, and slot coupling [8]. A compact 100×100 mm^2, quarter CDRA (Taconic CER-10 + FR27) has been designed to operate at 1.575 GHz (L1 band) with 60% bandwidth, 4.5 dBi gain, 72.89% efficiency, and $S_{11} < -15$ dB for GPS applications [9]. A compact triple-band hybrid CDRA (Alumina Ceramic) based on an FR4 sheet, fed by a microstrip line with concentric rings and partial ground plane to operate at 2.4/3.5/5.4 GHz with 26.6/20.4/18.67% bandwidths, 2.4/4.13/3.5 dBi gains, and $S_{11} < -35$ dB was reported for ISM/Wi-MAX/WLAN applications [10]. Likewise, a tri-band 100×100 mm^2 sized FR4-based square DRA (ECCOSTOCK HiK Rod) has been analyzed to work at 1.3/2.6/3.8 GHz with 19.5/6.58/8.2% bandwidth, 4.9/4.4/6.7 dBi gain, and $S_{11} < -15$ dB, respectively, for 4G/5G n77 applications [11]. An article proposed a quad-band 100×100 mm^2-sized square DRA (Alumina Ceramic) based on an FR4 sheet to work at 3.5/4/4.6/5 GHz with 4.31/5.61/5.01/4.32 dBi gains, and 71.73/76.24/74.31/64.04% efficiency, respectively, for 5G Sub-6 GHz applications [12]. Dwivedy et al. presented a penta-band semi-angular cylindrical DRA (alumina ceramic) on a 130×130 mm^2 FR4 sheet to resonate at 3.2/3.6/4.0/4.4/4.8 GHz with about 3.3 dBi gain, 45.1% bandwidth, and less than -10 dB return loss (S_{11}-dB) suitable for C-V2X and Sub-6 GHz applications [13]. A triple-band CDRA (alumina ceramic) array based on 120×120 mm^2 FR4 laminate was proposed to operate at 2.4/4.1/5.4 GHz

* Corresponding author: Kaushal Patel (kaushal.patel@bvmengineering.ac.in).

with 60% bandwidth, 9.0 dBi gain for Wi-Fi, wireless local area network (WLAN), and satellite applications [14]. An article reported the development of a CDRA (alumina ceramic) array based on $50 \times 40\,\text{mm}^2$ FR4 laminate to operate at 1.85 GHz, 5.13 GHz, 9.0 GHz, and 14.24 GHz frequencies with the peak gain of 1.20 dBi, 2.66 dBi, 3.91 dBi, 6.6 dBi, and 2.05 dBi, respectively, for multiband applications [15]. Various flower-shaped patch-based microstrip antennas using simple feeding techniques and a variety of footprints have been reported [16–18]. However, the existing single- and multi-band DRAs reveal large footprints, large DR (dielectric resonator) radiating area, unspecified radiation efficiency, and the usage of high-cost DR/substrate materials. The antenna miniaturization and performance enhancement can also be achieved by employing low-cost high-permittivity laminates, fractal geometries, split-ring resonators (SRRs), and modified ground plane geometries [18].

In this article, a novel low-cost, compact, and multiband flowerpot-shaped patch-based cylindrical dielectric resonator antenna (FPSDRA) is designed and analyzed. Here, CDR is excited by a combined microstrip line and tapered trapezoidal feedline. In the proposed antenna, a novel flowerpot-shaped patch radiator is introduced underneath the CDR to achieve multiband resonance, increase electrical peripheral path, and reduce surface current distribution. Later, a novel reduced ground plane has been implemented in the rear side of the dielectric substrate for impedance matching, antenna size reduction, and bandwidth enhancement. The proposed antenna prototype has been made using a low-cost FR4 substrate and alumina ceramic (Al_2O_3) based CDR. The proposed FPSDRA has achieved compactness of $65 \times 45\,\text{mm}^2$ to resonate at 1.54/2.02/3.23/3.95/5.54 GHz with the maximum gain of 4.32 dBi at 3.95 GHz, 98/92.51/83.59/87.15/85.56% respective radiation efficiency, adequate reflection coefficients (S_{11}) less than -15 dB, and adequate -10 dB impedance matching bandwidths suitable for Global Positioning System (GPS), Universal Mobile Telecommunications System (UMTS), Personal Communications Service (PCS), Wireless-Fidelity 5 (Wi-Fi5), Worldwide Interoperability for Microwave Access (WiMAX), NR Sub-6 GHz 5G, etc. applications. After comparing earlier research articles of different multiband DRAs made with different low-permittivity DR materials on standard dielectric substrates, feed techniques, and simple patch radiators, this presented work has introduced a novel compact and low-cost flowerpot-shaped patch radiator-based CDRA with reduced symmetrical octagonal hollowed-out ring edges excited by a combined microstrip-tapered trapezoidal feed structure integrated with reduced rectangular ground plane to offer penta-band operation with better reflection coefficients, peak gains, better radiation efficiency, and adequate radiation performance comparatively, which is considered as novelty in the proposed design. This article is organized sequentially as (2) antenna geometry design and configuration, (3) antenna electrical equivalent circuit, (4) the principle of operation and the role of antenna elements, (5) parametric analysis, (6) prototype and results discussion, and (7) conclusion.

2. ANTENNA GEOMETRY DESIGN AND ANTENNA CONFIGURATION

2.1. Antenna Geometry Design

The FPSDRA is shown in Fig. 1. The comprehensive antenna consists of a low-cost middle dielectric substrate layer, a feeding mechanism, and a novel patch radiator printed on the top surface of the middle substrate. The cylindrical DRA (CDRA) is mounted on the top of a patch radiator, and a rectangular ground is implemented in the bottom layer. Fig. 1 shows that the top layer consists of a flowerpot-shaped patch radiator comprising eight circular flower petals of radius — R_o and inter petal distance — P_L surrounding a center circular patch of radius — R_i based on a flower stem of slanted length — L_{FS}, widths — W_{S1} and W_{S2}, top loaded cylindrical dielectric resonator of radius — r_D, and height — h_D. Additionally, reduced octagonal hollowed-out ring edges of length — L_{OE}, width — W_{OE} are placed symmetrically at a distance W_{ES} from the flower stem to create a novel flowerpot-shaped patch radiator. Subsequently, the flowerpot-shaped radiator is excited by a novel combined microstrip line (50-Ω)-tapered trapezoidal feed structure of line length — L_F and line breadth — W_F, tapered trapezoidal feed base width — W_B, top width — W_T, slant edge length — L_T, and height — H_T. Furthermore, a reduced rectangular ground plane of length — L_G and width — W_G is implemented on the rear side of the dielectric laminate. The proposed prototype is simulated in microwave Computer Simulation Technology (CST) software.

The proposed FPSDRA can be accurately analyzed using a circular cavity model. The resonating modes sustained by the proposed antenna can be excited by forming a cylindrical DR, a radiating patch as a perturbed cavity, a dielectric substrate, and a reduced ground plane that forms a resonant cavity. The cavity model method is used to analyze and determine the electric field ($\overrightarrow{E_z}$) and magnetic field ($\overrightarrow{H_\emptyset}$) inside the cavity using the magnetic vector potential ($\overrightarrow{A_z}$) for TM_z modes as shown in Equation (1), which must satisfy the Helmholtz equation in cylindrical coordinates as shown in Equation (2) [19, 20]:

$$\overrightarrow{A_z} = B_{mnp} J_m(k_\rho \rho') \left[A_2 \cos(m\emptyset') + B_2 \sin(m\emptyset')\right] \cos(k_z z') \tag{1}$$

$$\nabla^2 \overrightarrow{A_z} + k^2 \overrightarrow{A_z} = 0 \tag{2}$$

where $k_\rho = \frac{X'_{mn}}{a}$, $k_z = \frac{p\pi}{h}$ and $m = p = 0, 1, 2, ..., n = 1, 2, 3...$

The primary cylindrical coordinates $\rho', \emptyset'$, and z' characterize the fields inside the cavities. The resonance frequencies of TM_{nmp} and TE_{nmp} modes can be determined using Equations (3) and (4), respectively [20]:

$$(f_r)_{nmp} = \frac{1}{2\pi\sqrt{\mu\varepsilon}} \sqrt{\left(\left(\frac{X_{mn}}{a}\right)^2 + \left(\frac{\pi p}{d}\right)^2\right)} \quad (\text{TM}_{nmp} \text{ mode}) \tag{3}$$

$$(f_r)_{nmp} = \frac{1}{2\pi\sqrt{\mu\pi}} \sqrt{\left(\left(\frac{X'_{mn}}{a}\right)^2 + \left(\frac{\pi p}{d}\right)^2\right)}$$

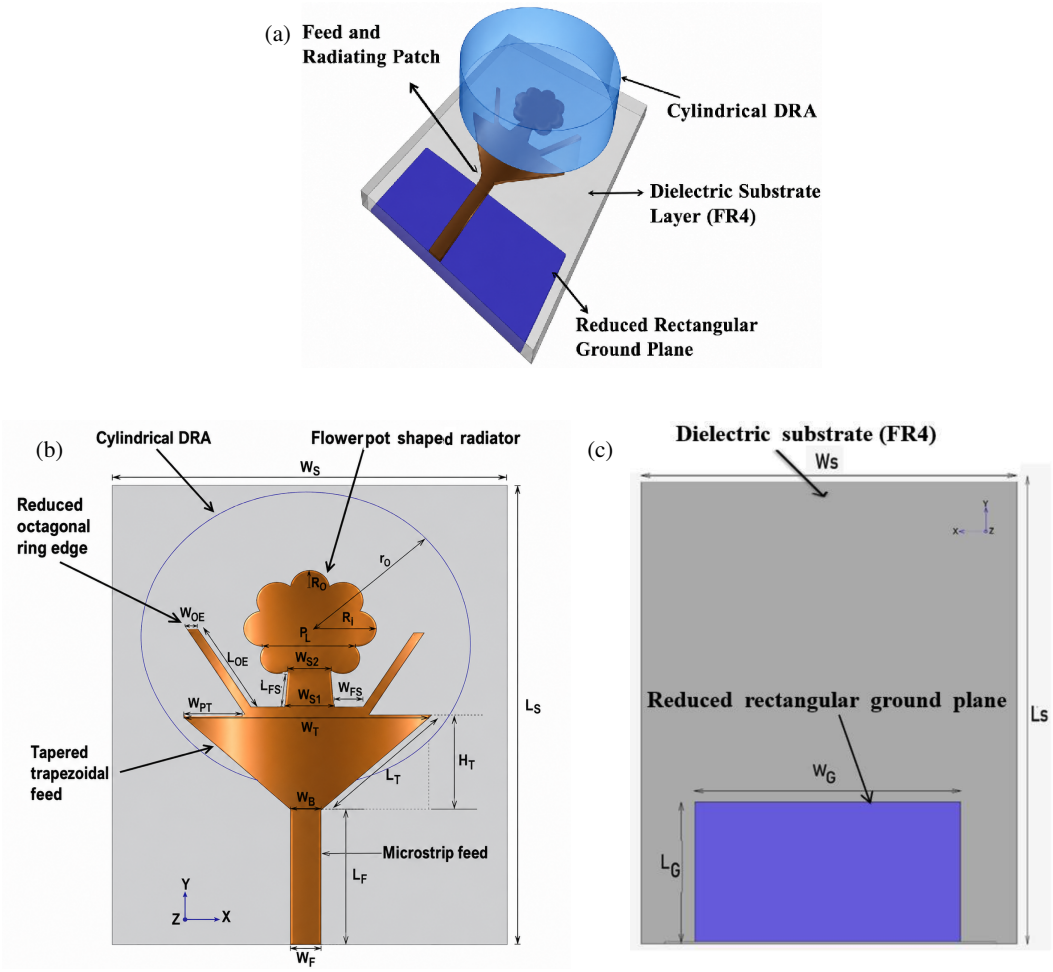

FIGURE 1. The proposed antenna design: (a) Isotropic view. (b) Topside view. (c) Rearside view.

$$(\mathrm{TE}_{nmp}\ \text{mode}) \tag{4}$$

Considering the factor of correction (F) owing to the fringing field effect, the actual circular patch radius (a) is replaced by an effective radius ($a_{eff} = R_i$ in cm), which can be calculated using Equations (5), (6), and (7) [11]:

$$a = \frac{F}{\left(\left\{1 + \frac{2h}{F\pi\varepsilon_r}\left(\left(\ln\left(\frac{F\pi}{2h} + 1.7726\right)\right)\right)\right\}\right)^{\frac{1}{2}}},$$

$$F = \frac{8.791 \times 10^9}{f_r \sqrt[2]{\varepsilon_r}} \tag{5}$$

$$a_{eff} = a\left\{1 + \frac{2h}{a\pi\varepsilon_r}\left[\ln\left(\frac{a\pi}{2h} + 1.7726\right)\right]\right\}^{\frac{1}{2}} \tag{6}$$

where h is the substrate height (in cm), f_r the resonance frequency (in Hz), and ε_r the dielectric substrate permittivity.

The cylindrical DRA dimensions can be calculated using Equation (7) [4]:

$$f_r = \frac{6.324 * c}{2\pi \sqrt[2]{\varepsilon_{\mathrm{DR}} + 2}}\left(0.27 + 0.36\left(\frac{r_D}{2h_D} + 1.7726\right) + 0.02\left(\frac{r_D}{2h_D}\right)^2\right) \tag{7}$$

where $c, f_r, \varepsilon_{\mathrm{DR}}, r_D$, and h_D are the speed of light (3×10^8 m/s), the resonance frequency (in Hz), the permittivity of CDR radius (in meter), and the height (in meter) of the CDR, respectively.

The octagonal ring edge effective length $L_{eff} = L_{OE}$ (in mm) can be calculated by using Equation (8) [21]:

$$L_{eff} = \frac{3 \times 10^8}{2 * f_r * \sqrt[2]{\varepsilon_{reff}}}, \qquad \varepsilon_{reff} = \frac{\varepsilon_r + 1}{2} \tag{8}$$

where f_r and ε_r are target resonance frequency (in GHz) and permittivity of the dielectric substrate, respectively.

The trapezoidal feed top (W_T) and base (W_B) widths (in mm) can be calculated by using Equation (9) [21]:

$$W_T = \frac{3 \times 10^8}{2 * f_r\,(\mathrm{GHz}) * \sqrt[2]{(\varepsilon_r + 1)/2}} = W_B \tag{9}$$

The antenna ground length (L_G) and width (W_G) can be calculated by using Equation (10) (all dimensions are in mm) [21]:

$$L_G = 6h + 2R_i, \quad W_G = 6h + (\pi/2)R_i \tag{10}$$

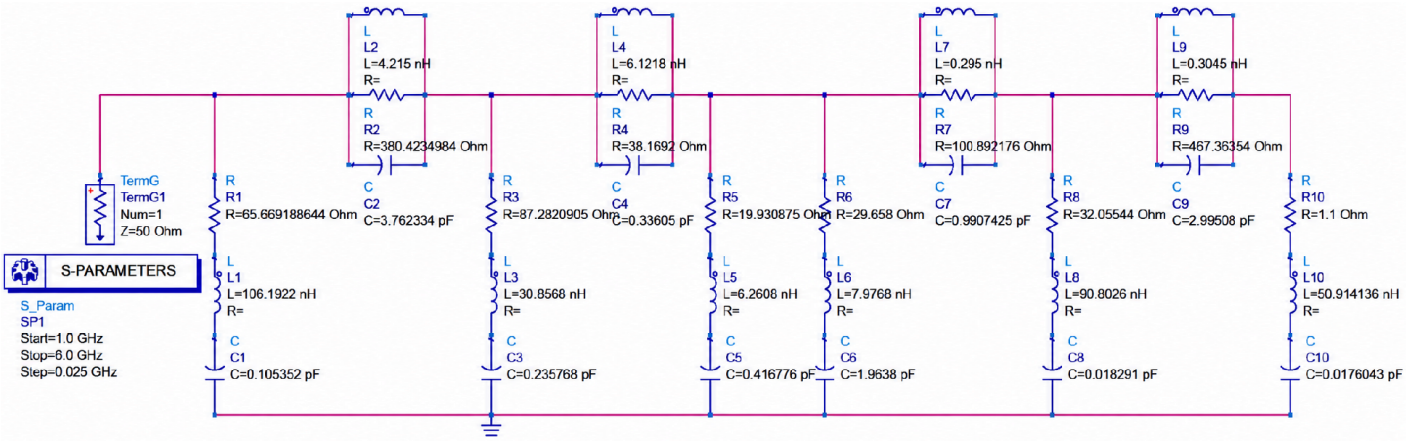

FIGURE 2. Antenna (RLC) equivalent circuit of the proposed antenna.

2.2. Antenna Configuration

The complete isometric view (a), top and rear side geometrical views (b) and (c) of the proposed antenna are revealed in Fig. 1. The non-planner antenna is made using a low-cost FR4 sheet ($\varepsilon_r = 4.4$, $\tan\delta = 0.02$) of $65 \times 45\,\text{mm}^2$ size. The full cylindrical dielectric resonator (CDR), fabricated using alumina ceramic material (Al_2O_3) with a radius $r_D = 21\,\text{mm}$ and height $h_D = 11\,\text{mm}$, is mounted on the topside of the flowerpot-shaped patch radiator. As shown in Fig. 1, the microstrip line is combined with a tapered trapezoidal shape transition feed and positioned from the top edge of the dielectric substrate to the middle of the flowerpot-shaped patch radiator for sufficient excitation. All the dimensional details are presented in Table 1.

TABLE 1. Proposed prototype parameter/dimensions in mm.

Parameter	Value (mm)	Parameter	Value (mm)
L_S	65	L_T	16.42
W_S	45	W_{PT}	5.99
H_S	1.6	L_{OE}	11.98
L_F	20	W_{OE}	1.0
W_F	3.0	W_{S1}	4.74
W_B	3.0	W_{S2}	4.24
H_T	12.7	W_{ES}	3.13
r_D	21	P_L	10.23
h_D	11	W_T	24
R_i	14.47	R_o	2.12

3. ANTENNA ELECTRICAL EQUIVALENT CIRCUIT

A lumped-element antenna equivalent circuit model of the proposed antenna is presented in Fig. 2 to explain its functionality. A 50-Ω resistor in the antenna equivalent circuit model represents the suitably matched transmission line used for effective power transfer, characteristic impedance, and impedance matching. The series RLC circuit made by $R1, L1, C1$ indicates a CDRA responsible for 1.54 GHz resonance frequency (F_{r1}), and a series RLC circuit made by $R5, L5, C5$ indicates that the center circular patch radiator is responsible for 2.02 GHz resonance frequency (F_{r2}). The series RLC circuit made by $R6, L6, C6$ indicates symmetrical octagonal ring side edges responsible for 3.23 GHz resonance frequency (F_{r3}), and series RLC circuits made by $R8, L8, C8$ and $R10, L10, C10$ lumped elements denote coupled circular petals responsible for 3.95 GHz (F_{r4}) and 5.54 GHz (F_{r5}) resonance frequency, respectively. Remaining shunt RLC circuits show non-resonating 1.68 GHz, 2.65 GHz, 4.63 GHz, 5.24 GHz frequencies. Likewise, the series RLC circuit made by $R8, L8, C8$ shows non-resonating 5.03 GHz. Here, all R lumped values signify electromagnetic (EM) fields formed by current flows; C values signify conduction and radiation losses; L values signify the energy kept in E-fields. Therefore, to optimize the antenna performance, (i) decrease the resistance (R) values to increase the antenna efficiency and the radiated power; (ii) adjusting L and C values can fine-tune the resonance frequency and impedance matching bandwidths [22]. The circuit is realized in advanced design system (ADS) software, as shown in Fig 2, and the ADS estimated values of the equivalent circuit R,L,C lumped components are presented in Table 2. The reflection coefficients (S_{11}-dB) obtained from CST and ADS software are found in good agreement, as shown in Fig. 3.

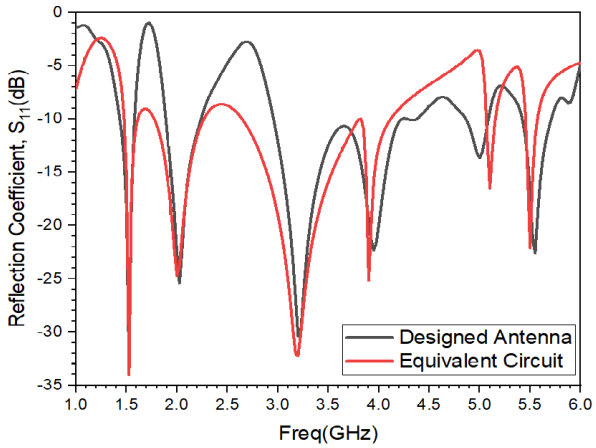

FIGURE 3. Simulated graph of S_{11}-dB matched in CST and ADS software.

TABLE 2. RLC lumped values of equivalent circuit model.

Resonance Frequency (F_r-GHz)	R-Values (Ω) (Tuned Estimated)	L-Values (nH) (Tuned Estimated)	C-Values (pF) (Tuned Estimated)
$F_{r1} = 1.54$	$R1 = 65.66918$	$L1 = 106.1922$	$C1 = 0.105352$
$F_{r2} = 2.02$	$R3 = 87.28209$	$L3 = 30.8528$	$C3 = 0.33605$
$F_{r3} = 3.23$	$R5 = 19.9308$	$L5 = 6.2608$	$C5 = 0.416776$
$F_{r4} = 3.95$	$R6 = 29.658$	$L6 = 7.9768$	$C6 = 1.9638$
$F_{r5} = 5.54$	$R10 = 1.1$	$L10 = 50.9141$	$C10 = 0.0176$

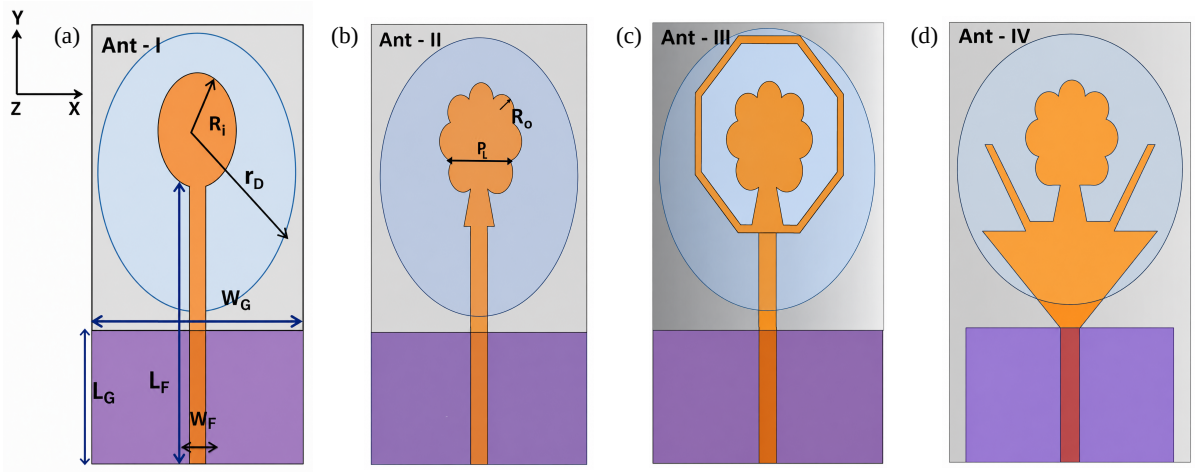

FIGURE 4. Designs of reference antenna (a) case-I, (b) case-II, (c) case-III, (d) case-IV.

4. PRINCIPLE OF OPERATION AND THE ROLE OF ANTENNA ELEMENTS

The working principle of the proposed FPSDRA is discussed in this section. During the design, preliminary research, and analysis process, a (non-modified) center circular patch of radius (R_i) was initially made on the top of the substrate, with a whole rectangular ground plane on the back side of the substrate with a copper cladding of thickness ($t = 0.035$ mm) excited by a simple microstrip line feed, and loaded with a cylindrical DR on the top of the circular patch in antenna case-I prototype as shown in Fig. 4(a). Subsequently, in the antenna case-II design, small circular flower petals of radius (R_o) are employed on the peripheral edges of the patch as fractal shapes along with flower stem based feeding to enhance surface current distribution, impedance matching, and multiband low to high frequency resonance, as shown in Fig. 4(b). Later, in antenna case-III, a hollowed-out octagonal ring-shape coupled radiator was introduced surrounding the flower petals-stem shape to add new resonance peaks, as shown in Fig. 4(c). Finally, in antenna case-IV design, a tapered trapezoidal feed is employed in between the microstrip feed and flower stem feed for gradual current transition and stable multiband resonance. Eight edges of octagonal ring-shaped radiator have been reduced to two symmetrical edges for surface current reduction, excess current reduction, surplus resonance, and extreme directional pattern. Additionally, the full rectangular ground plane is reduced on the rear side of the dielectric substrate for antenna size reduction and impedance bandwidth enhancement, as shown in Fig. 4(d). Fig. 5 shows the simulated reflection coefficients (S_{11}-dB) of the four referral antenna cases. From Fig. 4, it can be seen that owing to the CDR, a 1.54 GHz resonance mode is perceived, owing to the flower-shaped patch radiator maximum dimension from center 2.02 GHz resonance mode, and owing to reduced symmetrical octagonal ring side edges, 3.23 GHz resonance mode is perceived. Moreover, two remaining resonant modes are perceived at 3.95 GHz and 5.54 GHz, owing to flower petals and the coupling between petals of radius R_o (in mm) $= \frac{P_{L\,(\mathrm{mm})}}{4}$ [13].

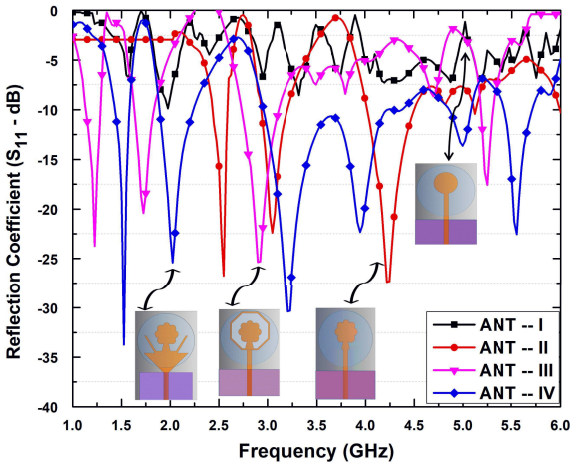

FIGURE 5. Simulation results of the reflection coefficient (S_{11}-dB) for referral antenna cases.

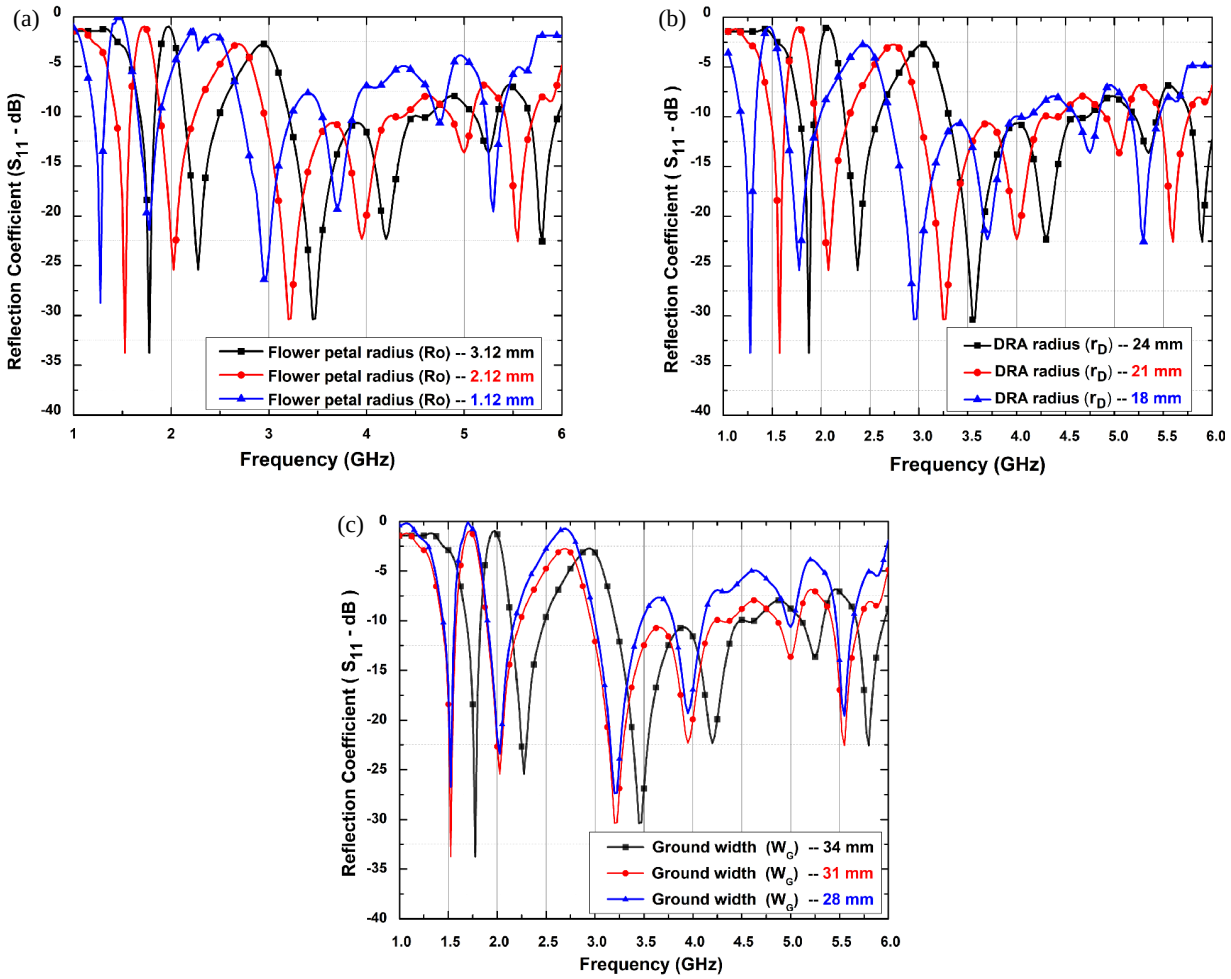

FIGURE 6. Simulation of parametric analysis for variation in (a) flower petal radius (R_o), (b) CDRA radius (r_D), (c) rectangular ground plane width (W_G).

5. PARAMETRIC ANALYSIS

The parametric analysis was performed by changing the circular flower petal radius (R_o), CDRA radius (r_D), and rectangular ground plane width (W_G). Fig. 6(a) shows the effect of the flower petal radius (R_o) on the reflection coefficients (S_{11}-dB). By increasing and decreasing the flower petal radius, due to the change in the electrical length of the overall antenna, the resonance notch can be shifted towards lower and higher frequencies, respectively. Here, R_o was tuned between 1.12 mm and 3.12 mm, and the desired resonance notches with optimum reflection coefficients were obtained at 2.12 mm. Fig. 6(b) shows the effect of CDRA radius (r_D) on the reflection coefficient (S_{11}-dB). By increasing and decreasing the CDRA radius, due to the change in electrical length and the coupling of energy, resonance notches can be shifted towards lower and higher bands, respectively. The CDR radius (r_D) is tuned by 18 mm, 21 mm, and 24 mm. Finally, the desired notches with optimum reflection coefficients were obtained at 21 mm. Fig. 6(c) shows the effect of the rectangular ground plane width (W_G). The ground plane width was tuned from 28 mm to 34 mm. It is observed that owing to the change in capacitance, surface current distribution, and edge interference, the desired multiband resonance with optimum reflection coefficients and bandwidths is obtained at $W_G = 31$ mm.

6. PROTOTYPE AND RESULTS DISCUSSION

After the effective parametric analysis, significant dimensions of the antenna were determined for the prototype design. Subsequently, the prototype was fabricated and tested in an anechoic chamber (800 MHz to 18 GHz) as shown in Fig. 7. The proposed multiband FPSDRA is built using a dielectric laminate of FR4.

Subsequently, the flowerpot-shaped patch radiator was etched and excited by a combined microstrip-line-tapered trapezoidal feed line on the topside of the FR4 substrate.

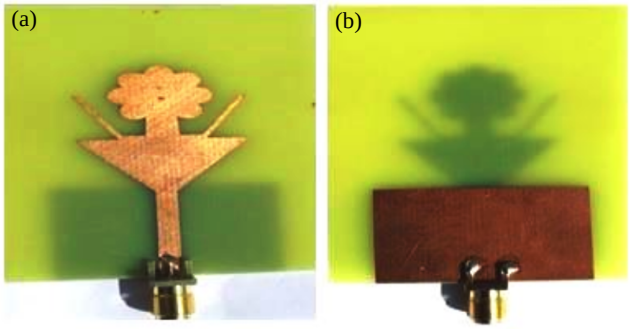

FIGURE 7. (a) Top view of fabricated substrate and (b) bottom view of the fabricated substrate.

FIGURE 8. Proposed assembled antenna prototype topmost view.

Finally, a cylindrical DRA (Al_2O_3, $\varepsilon_{DR} = 9.8$) is attached to the top of the patch radiator. This feed line is excited by an RF SMA jack connector (50-Ω) as shown in Fig. 8. During the testing, a slight inconsistency was observed between material properties and built-up tolerances, signal degradation caused by cables and connectors, thickness and quality of the adhesive used to attach the CDR on the antenna plane, as shown in Fig. 8. The reflection coefficients, peak gains, and radiation patterns were measured using a reference horn antenna measurement setup in an anechoic chamber, as shown in Fig. 9.

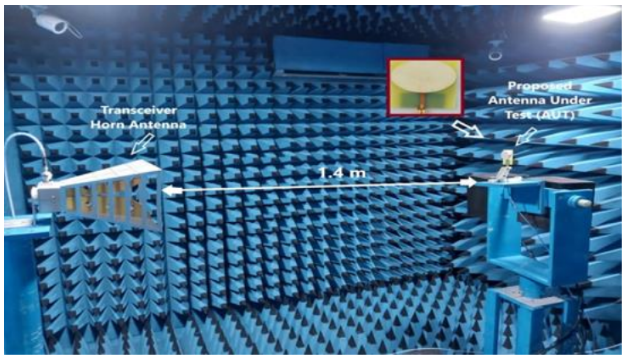

FIGURE 9. Anechoic chamber test and measurement setup.

Figure 10 shows the simulated and measured reflection coefficients (S_{11}-dB). The simulated and measured reflection coefficients are < -30 dB at 1.54 GHz, < -20 dB at 2.02 GHz, < -20 dB at 3.23 GHz, < -19 dB at 3.95 GHz and 5.54 GHz. In Fig. 10, absolute bandwidths are shown as BAND1 to BAND5, whereas Table 3 shows -10 dB impedance matching bandwidths in percentage. As shown in Fig. 12, the proposed antenna provides adequate agreement between the simulated and experimentally measured voltage standing wave ratios (VSWRs) obtained around ∼2 with $< 5\%$ deviance owing to fabrication tolerances, SMA connector stray effects, dielectric material property variations and losses, copper conductor losses, and experimental environment reflections. The evaluation between the simulated and measured peak gains

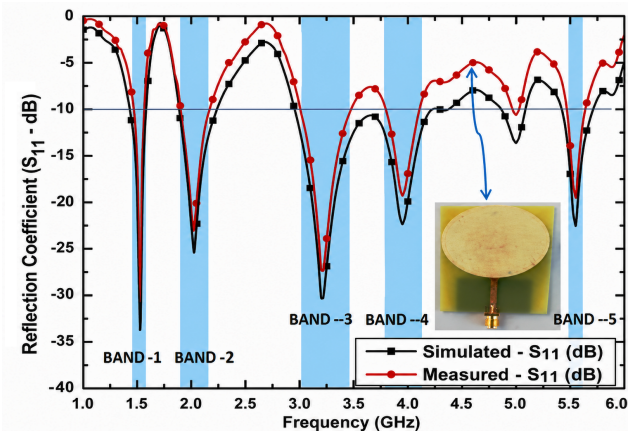

FIGURE 10. Simulated and measured results of reflection coefficients (S_{11}-dB).

is depicted in Fig. 13 with convincing agreement. The measured peak gains are 2.01 dBi, 2.05 dBi, 3.02 dBi, 4.85 dBi, and 2.24 dBi at 1.54 GHz, 2.02 GHz, 3.23 GHz, 3.95 GHz, and 5.54 GHz, respectively. The discrepancy between the simulated and measured gains is due to substantial feed, connector, and cable losses. The simulated radiation efficiencies are 98.12%, 92.51%, 83.60%, 87.15%, and 85.59% for respective bands, as shown in Fig. 13. Additionally, in this design, the fractional power losses associated with the CDR and the remaining antenna structure are calculated using the accepted input power (P_{in}), radiated power (P_{rad}), conductor loss, and dielectric loss. The simulated fraction power losses in CDR are 0.01/0.01/0.02/0.02/0.03%, and those of the remaining part of the antenna structure are 1.99/7.48/16.39/12.87/14.38% at 1.54/2.02/3.23/3.95/5.54 GHz, respectively.

Figure 11 shows the E-field distributions of the simulated antenna geometry at 1.54 GHz, 2.02 GHz, 3.23 GHz, 3.95 GHz, and 5.54 GHz, respectively. It indicates high current density at different elements of the antenna geometry. Fig. 14 shows simulated and measured radiation 2D polar plots of E-plane (xz-plane) and H-plane (yz-plane) at 1.54 GHz, 2.02 GHz, 3.23 GHz, 3.95 GHz, and 5.54 GHz. These radiation plots have attained adequate gains in the boresight direction due to the variation in the dimensions of the ground plane, tapered trapezoidal feed, and CDRA.

Table 3 shows a comparison of the proposed prototype with earlier designs in terms of several antenna performance parameters, such as resonating frequencies, operating bands, DR properties, type of dielectric laminates, size of antenna, S_{11}, and gain for L1/S/C band applications. Compared to the prior designs, the proposed multiband antenna is compact and has low cost, employing a novel flowerpot-shaped patch radiator excited by a combined microstrip-tapered trapezoidal feed structure, integrated with a reduced ground plane and a low-cost cylindrical dielectric resonator. Moreover, this new design offers adequate results in terms of reflection coefficients (S_{11}-dB), peak gains, -10 dB impedance bandwidths (%), radiation features, and radiation efficiencies for mentioned applications. Finally, the proposed prototype is suitable for 5G-enabled GNSS (5GNSS, 1.48–1.59 GHz), state of the art wireless applications, such as UMTS 2100/PCS 1900 (1.88–2.21 GHz), Wi-

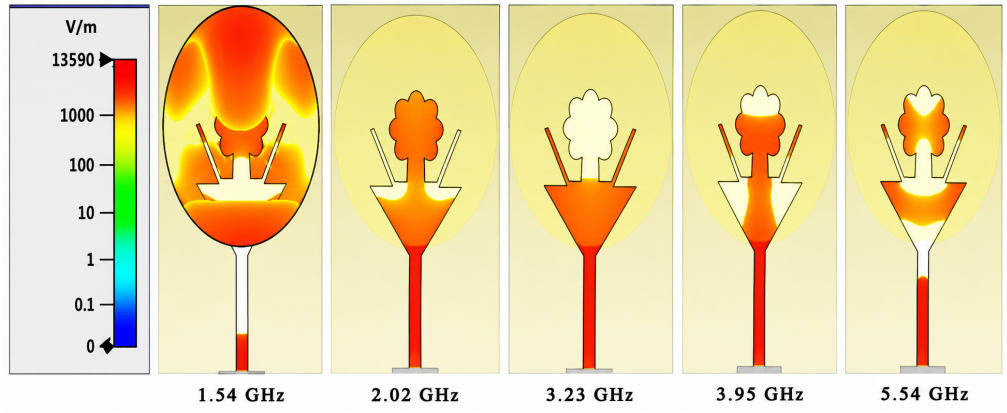

FIGURE 11. E-field distributions at 1.54 GHz, 2.02 GHz, 3.23 GHz, 3.95 GHz, and 5.54 GHz.

TABLE 3. Comparison assessment of the proposed DRA prototype with earlier DRA prototypes.

Ref.	F_r (GHz)	Operating Bands	DR Material (ε_{DR})	Antenna Size (mm^2) and Dielectric Substrate (ε_r)	DR Size (mm) (Shape)	S_{11} (dB)	VSWR	Gain (dBi)	-10 dB BW (%)	Radiation Efficiency (%)
[9]	1.57	1.56–1.58 (Single-band)	Taconic CER10 + FR 27 (12)	100×100 Taconic CER-10 (10)	$D = 38.6$ $H = 6.46$ (Quarter CDRA)	-15	1.0	4.50	60	72.89
[10]	2.4 3.5 5.4	1.98–2.59 3.24–3.85 4.85–5.85 (Tri-band)	Alumina Ceramic (9.8)	50×50 FR4 (4.4)	$D = 23.5$ $H = 9.0$ (Hybrid CDRA)	< -40 < -35 < -30	NM	2.40 4.13 3.5	26.6 20.4 18.6	NM
[11]	1.3 2.6 3.8	1.67–2.07 2.50–2.67 3.50–3.80 (Tri-band)	ECCOSTOCK Hik Rod (10)	64×85 FR4 (4.4)	$L = 40$ $W = 40$ $H = 21$ (Square DRA)	< -20 < -15 < -20	< 2 < 2 < 2	4.9 4.4 6.7	19.5 6.58 8.2	81 72.7 73.5
[12]	3.5 4.0 4.6 5.0	3.3–4.2 3.3–4.2 4.4–5.0 4.4–5.0 (Quad-band)	Alumina Ceramic (9.8)	100×100 FR4 (4.4)	$L = 44$ $W = 44$ $H = 17$ (Square DRA)	-10.10 -16.92 -22.85 -12.85	NM	4.31 5.61 5.01 4.32	NM	71.73 76.24 74.31 64.04
[13]	3.2 3.6 4.0 4.4 4.8	3.18–5.01 (Penta-band)	Alumina Ceramic (9.8)	130×130 FR4 (4.4)	$D = 44$ $H =$ NM (Semi angular DRA)	< -10 < -10 < -10 < -10 < -10	< 2 < 2 < 2 < 2 < 2	$\sim$3.3	45.1	NM
This work	1.54 2.02 3.23 3.95 5.54	1.48–1.59 1.88–2.21 2.95–4.21 2.98–4.21 5.42–5.64 (Penta-band)	Alumina Ceramic (9.8)	65×45 FR4 (4.4)	$D = 42$ $H = 11$ (Cylindrical DRA)	-33.73 -25.40 -30.37 -22.32 -22.55	1.12 1.23 1.34 1.45 1.56	2.17 2.35 3.30 5.11 2.54	9.45 7.12 21.08 13.79 5.24	98.00 92.51 83.59 87.15 85.56

(NM = Not mentioned, D = Diameter, H = Height)

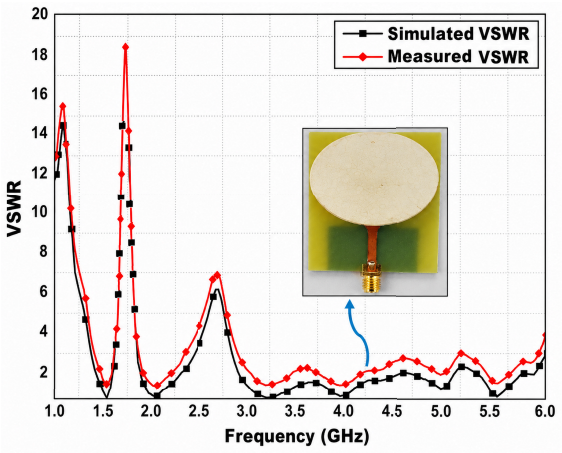

FIGURE 12. Simulated and measured VSWRs.

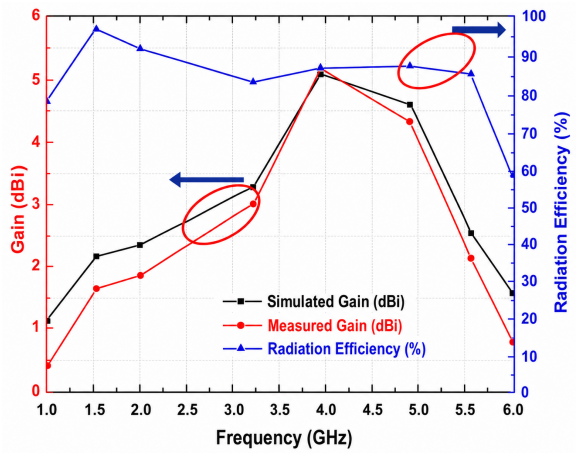

FIGURE 13. Simulated and measured peak gains and simulated radiation efficiencies.

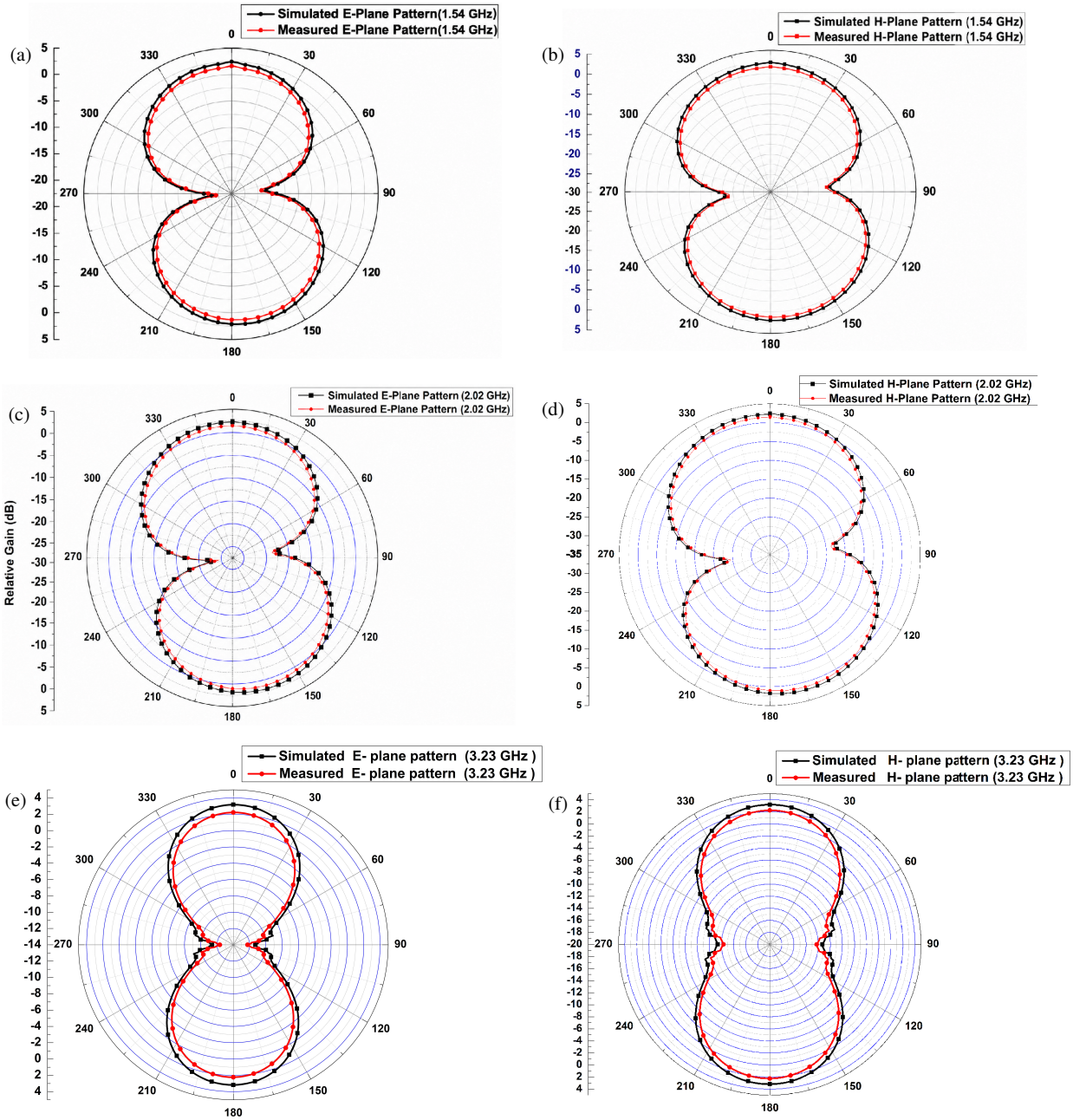

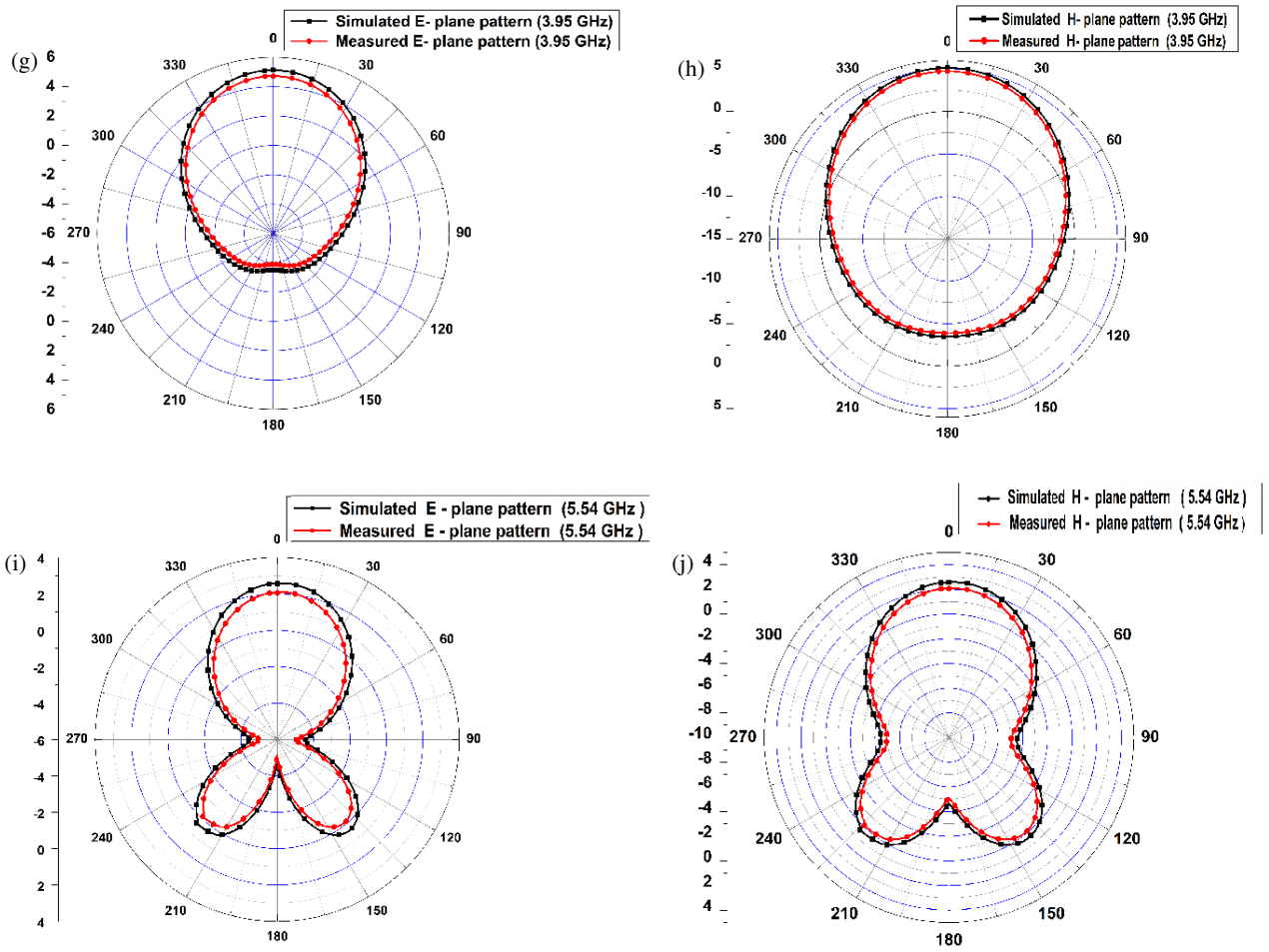

FIGURE 14. Simulated and measured radiation plots of (a), (c), (e), (g), (i) E-plane and (b), (d), (f), (h), (j) H-plane at 1.54 GHz, 2.02 GHz, 3.23 GHz, 3.95 GHz, and 5.54 GHz, respectively.

Fi 5 (2.98–4.21 GHz), WiMAX (2.98–3.65 GHz), and n77/78 Sub-6 GHz 5G (5.42–5.64 GHz) applications. In the future, researchers may improve axial ratio and increase gains using array structures for next-generation wireless applications.

7. CONCLUSION

A new miniaturized multiband cylindrical dielectric resonator antenna (CDRA) based on a flowerpot-shaped patch radiator was designed, simulated, fabricated, and tested. The proposed antenna is excited using a combined microstrip-tapered trapezoidal feed structure and employs a reduced rectangular ground plane on the rear side of a low-cost FR4 laminate. A low-permittivity, low-cost cylindrical dielectric resonator (DR) is utilized to generate lower- and higher-order resonances. The reduced ground plane has reduced the antenna size and improved the radiation patterns, whereas the novel flowerpot-shaped radiator enhanced the multiband resonance. The cylindrical DR, the center circular patch of the flower-shaped patch, symmetrical reduced octagonal ring edges, and coupling between flower petals have provided resonating notches at 1.54 GHz, 2.02 GHz, 3.23 GHz, 3.95 GHz, and 5.54 GHz, respectively. The proposed prototype offers adequate reflection coefficients, gains, -10 dB impedance matching bandwidths (%), and radiation performance for 5GNSS (GPS), UMTS, PCS, Wi-Fi5, WiMAX, and n77/78 Sub-6 GHz 5G applications.

ACKNOWLEDGEMENT

The authors are grateful to Electromagnetics and Antenna Research Centre (ELARC) at Birla Vishvakarma Mahavidyalaya, Vallabh Vidyanagar, Anand, Gujarat for providing the prototype testing and measurement facility.

REFERENCES

[1] Petosa, A., A. Ittipiboon, Y. M. M. Antar, D. Roscoe, and M. Cuhaci, "Recent advances in dielectric-resonator antenna technology," *IEEE Antennas and Propagation Magazine*, Vol. 40, No. 3, 35–48, 1998.

[2] Chen, H.-D., Y.-C. Tsai, C.-Y.-D. Sim, and C. Kuo, "Broadband eight-antenna array design for sub-6 GHz 5G NR bands metal-frame smartphone applications," *IEEE Antennas and Wireless Propagation Letters*, Vol. 19, No. 7, 1078–1082, 2020.

[3] Petosa, A. and A. Ittipiboon, "Dielectric resonator antennas: A historical review and the current state of the art," *IEEE Antennas and Propagation Magazine*, Vol. 52, No. 5, 91–116, 2010.

[4] Petosa, A., *Dielectric Resonator Antenna Handbook*, Artech House, Boston/London, 2007.

[5] Luk, K. M. and K. W. Leung, *Dielectric Resonator Antennas*, Research Studies Press, 2003.

[6] Prajapati, P., M. Anand, A. Jadav, and R. Joshi, "Design of single feed compact circularly polarized dual band dielectric resonator antenna for L5 and S bands applications," in *2023 IEEE Wireless Antenna and Microwave Symposium (WAMS)*, 1–5, Ahmedabad, India, 2023.

[7] Drossos, G., Z. Wu, and L. E. Davis, "Theoretical and experimental investigation of cylindrical dielectric resonator antennas," *Microwave and Optical Technology Letters*, Vol. 13, No. 3, 119–123, 1996.

[8] Long, S., M. McAllister, and L. Shen, "The resonant cylindrical dielectric cavity antenna," *IEEE Transactions on Antennas and Propagation*, Vol. 31, No. 3, 406–412, 1983.

[9] Paulena, G. P., J. M. Vieira, A.-H. A. A. Bouari, E. R. Schlosser, and M. V. T. Heckler, "Compact top-loaded quarter-cylinder dielectric resonator antenna," *Journal of Microwaves, Optoelectronics and Electromagnetic Applications*, Vol. 24, No. 2, e2025292093, 2025.

[10] Rao, L. N., G. Immadi, and M. V. Narayana, "Design of tri-band hybrid dielectric resonator antenna for wireless applications," *Progress In Electromagnetics Research Letters*, Vol. 98, 75–84, 2021.

[11] Cheh Lin, I. K., M. H. Jamaluddin, and A. Gaya, "A triple band substrate integrated waveguide with dielectric resonator antenna for 4G and 5G applications," *Micromachines*, Vol. 14, No. 7, 1284, 2023.

[12] Bazadry, N. A., H. A. Rahim, M. N. M. Yasin, and M. Abdulmalek, "Quadruple band MIMO dielectric resonator antenna for 5G sub-6 GHz applications," *Indonesian Journal of Electrical Engineering and Computer Science*, Vol. 28, No. 3, 1554–1562, 2022.

[13] Dwivedy, B., T. K. Das, D. K. Mahapatra, and D. Gayen, "A semi-angular cylindrical shape based wideband circularly polarized dielectric resonator antenna for C-V2X and sub-6 GHz IoT applications," *IEEE Access*, Vol. 13, 106 218–106 229, 2025.

[14] Vahora, A. and K. Pandya, "Implementation of cylindrical dielectric resonator antenna array for Wi-Fi/wireless LAN/satellite applications," *Progress In Electromagnetics Research M*, Vol. 90, 157–166, 2020.

[15] Pandya, K., T. Upadhyaya, U. Patel, R. Pandey, and A. Pandya, "Dielectric resonator antenna array development for GSM 1800/WLAN/radar/direct broadcast satellite applications," in *Proceedings of the International Conference on IoT Based Control Networks & Intelligent Systems — ICICNIS 2021*, Kerala, India, 2021.

[16] Gupta, N., J. Saxena, and K. S. Bhatia, "Design of wideband flower-shaped microstrip patch antenna for portable applications," *Wireless Personal Communications*, Vol. 109, No. 1, 17–30, 2019.

[17] Sharma, M., Y. K. Awasthi, H. Singh, R. Kumar, and S. Kumari, "Compact UWB antenna with high rejection triple band-notch characteristics for wireless applications," *Wireless Personal Communications*, Vol. 97, No. 3, 4129–4143, 2017.

[18] Patel, U., T. Upadhyaya, V. Sorathiya, K. Pandya, A. Alwabli, K. Dave, N. F. Soliman, and W. El-Shafai, "Split ring resonator geometry inspired crossed flower shaped fractal antenna for satellite and 5G communication applications," *Results in Engineering*, Vol. 22, 102110, 2024.

[19] Patel, D. H. and G. D. Makwana, "Multiband antenna for GPS, IRNSS, sub-6 GHz 5G and WLAN applications," *Progress In Electromagnetics Research M*, Vol. 116, 53–63, 2023.

[20] Chew, W. C., *Lectures on Electromagnetic Field Theory*, Purdue University, 2020.

[21] Balanis, C. A., *Antenna Theory: Analysis and Design*, 3rd ed., Wiley India Pvt. Ltd., 2005.

[22] Thereja, B. L., *Basic Electrical Engineering*, Tata McGraw Hill, 2000.